Open Access

Leyma P. De Haro[a], Todor Karaulanov[a], Erika C. Vreeland[a], Bill Anderson, Helen J. Hathaway, Dale L. Huber, Andrei N. Matlashov, Christopher P. Nettles, Andrew D. Price, Todd C. Monson and Edward R. Flynn[a],*

Magnetic relaxometry as applied to sensitive cancer detection and localization

Abstract

Background: Here we describe superparamagnetic relaxometry (SPMR), a technology that utilizes highly sensitive magnetic sensors and superparamagnetic nanoparticles for cancer detection. Using SPMR, we sensitively and specifically detect nanoparticles conjugated to biomarkers for various types of cancer. SPMR offers high contrast *in vivo*, as there is no superparamagnetic background, and bones and tissue are transparent to the magnetic fields.

Methods: In SPMR measurements, a brief magnetizing pulse is used to align superparamagnetic nanoparticles of a discrete size. Following the pulse, an array of superconducting quantum interference detectors (SQUID) sensors detect the decaying magnetization field. NP size is chosen so that, when bound, the induced field decays in seconds. They are functionalized with specific biomarkers and incubated with cancer cells *in vitro* to determine specificity and cell binding. For *in vivo* experiments, functionalized NPs are injected into mice with xenograft tumors, and field maps are generated to localize tumor sites.

Results: Superparamagnetic NPs developed here have small size dispersion. Cell incubation studies measure specificity for different cell lines and antibodies with very high contrast. *In vivo* animal measurements verify SPMR localization of tumors. Our results indicate that SPMR possesses sensitivity more than 2 orders of magnitude better than previously reported.

Keywords: cancer; magnetic relaxometry; nanoparticles; SQUID.

[a]These authors contributed equally to this work.

*Corresponding author: Edward R. Flynn, Senior Scientific, LLC, 800 Bradbury SE, Albuquerque, NM 87106, USA,
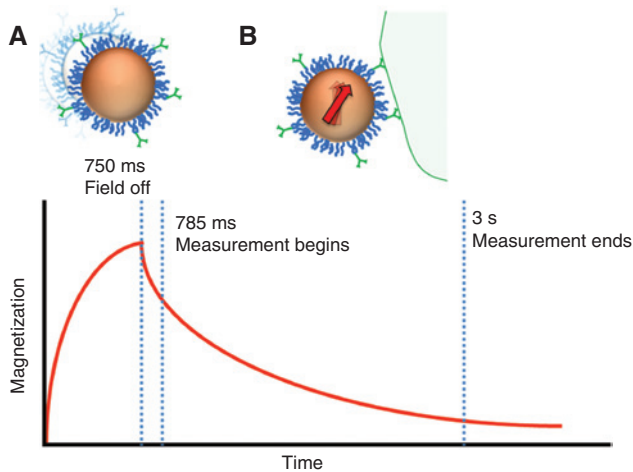E-mail: seniorsci@erfmaf.com; erflynn@erfmaf.com
Leyma P. De Haro, Todor Karaulanov, Erika C. Vreeland, Bill Anderson, Christopher P. Nettles and Andrew D. Price: Senior Scientific LLC, Albuquerque, NM, USA
Helen J. Hathaway: Department of Cell Biology and Physiology, University of New Mexico School of Medicine, Albuquerque, NM, USA
Dale L. Huber: Center for Integrated Nanotechnologies, Sandia National Laboratories, Albuquerque, NM, USA
Andrei N. Matlashov: Los Alamos National Laboratory, Group of Applied Modern Physics, Los Alamos, NM, USA
Todd C. Monson: Sandia National Laboratories. Nanoscale Sciences Department, Albuquerque, NM, USA

Introduction

Superparamagnetic relaxometry (SPMR) is a technique that combines the use of sensitive magnetic sensors and the superparamagnetic properties of magnetite (Fe_3O_4) nanoparticles (NPs). SPMR is an emerging technology [8, 9, 16] with several potential applications, particularly in cancer research, where the functionalization of NPs with biomarkers allows specific binding to cancer cells. The unique behavior of superparamagnetic NPs provides high contrast between bound and unbound NPs. This method has been shown to be extremely sensitive for detection of cancer cells; e.g., SPMR is several orders of magnitude more sensitive than a mammogram [11].

The basic mechanism of the SPMR measurement is illustrated in Figure 1. Antibody functionalized superparamagnetic magnetite NPs are introduced to a sample containing the target tissue. Next, a small magnetizing pulse is applied to the area of interest; the field is then switched off, and after a short dead time, the relaxation of NP magnetization is detected by the SQUID sensor array. Relaxation of the induced moments can take place by one of two mechanisms: Brownian motion of unbound particles through the surrounding medium, or Néel relaxation [18] of particles bound to cells, whereby relaxation

Figure 1: The MRX measurement.
At t=0, a 4-mT field is applied to align the magnetization vector of the nanoparticles (NPs) with the z-axis of the instrument. After 750 ms, the field is switched off and, following 35 ms of dead time, the superparamagnetic relaxometry (SPMR) measurement begins. After 2.2 s, the measurement ends. (A) NPs experiencing Brownian motion relax quickly, before the onset of the measurement, and are not detected. (B) Néel relaxation occurs relatively slowly, so only NPs bound to cells are detected during the measurement period.

occurs by reorientation of the electron orbits within the NPs. Néel relaxation has a strong (exponential) dependence on the particle volume, so it is critical that the NP diameter falls within a narrow range, approximately 24–26 nm, to ensure that the relaxation is detectable on the timescale of the measurement [2]. For 24–26 nm Fe_3O_4 NPs in a physiological medium, Brownian and Néel processes occur on substantially different time scales. The significance of this phenomenon *in vivo* is that bound particles can be distinguished from unbound particles. In the studies presented here, we focus on the results obtained with commercially available Fe_3O_4 NPs (Ocean NanoTech, SHP and SPP series). We also undertook studies using in-house manufactured NPs (Senior Scientific), with significantly improved properties (lower shape/size dispersity, increased magnetic susceptibility, increased batch reproducibility) to demonstrate improved sensitivity (detected moment/kg Fe) of the SPMR technique.

SPMR requires sensors capable of detecting fields at the picoTesla (pT) level, on the scale of the fields emitted by NPs during the relaxation process. The high sensitivity of SQUID detectors [20] have made them the predominant sensors in SPMR systems, although they have also been utilized extensively for measuring magnetic fields emitted by the brain and heart [4, 5, 10]. Arrangement of the sensors into arrays allows spatial maps of the emitted fields to be generated. Localization of the NP sources can

then be performed by fitting a dipolar model [10, 12] to the acquired data using a quasi-static approximation. More recently, fluxgate sensors [17] and atomic magnetometers [7, 14, 15] have also been employed for sensitive detection of magnetic fields in SPMR experiments. Incorporation of gradiometers allow fields from distant sources to be cancelled, thus making it possible for SPMR measurements to be performed in unshielded environments.

The utility of SPMR is specific and provides sensitive localization of NPs bound to cancer cells. It differs from MRI, which produces an anatomical image of the subject through measurement of the spins of hydrogen atoms in tissue without specificity to cell phenotype. In the presence of cancerous tumors in the body, SPMR yields a definitive localization of the NPs bound to cancer cells with sub-millimeter accuracy and high contrast. The contrast generated by NPs in MRI would be greatly diminished by comparison, as only small perturbations of the local field caused by the NPs can be measured. In some regards, SPMR can be compared to positron emission tomography (PET) methods; SPMR measures emitted magnetic fields from the relaxation of bound NPs, whereas PET measures emitted gamma rays from the annihilation of positrons. However, the resolution of PET is limited by the positron path uncertainty before annihilation and scattering of the gamma rays in intervening tissue, whereas SPMR resolution is determined by the number of magnetic field measurement points and the inverse electromagnetic solution. The magnetic fields used in SPMR measurements are transparent to tissue and bone. Furthermore, SPMR technology does not use ionizing radiation and applies magnetic fields approximately 1% of those used in an MRI measurement. Unlike other contrast agents (such as radioactive tracers used in PET scans or gadolinium used in MRI), Fe_3O_4 is not inherently toxic. Here, we show that SPMR offers a novel way to specifically and sensitively quantify small numbers of cancer cells *in vitro* and *in vivo*.
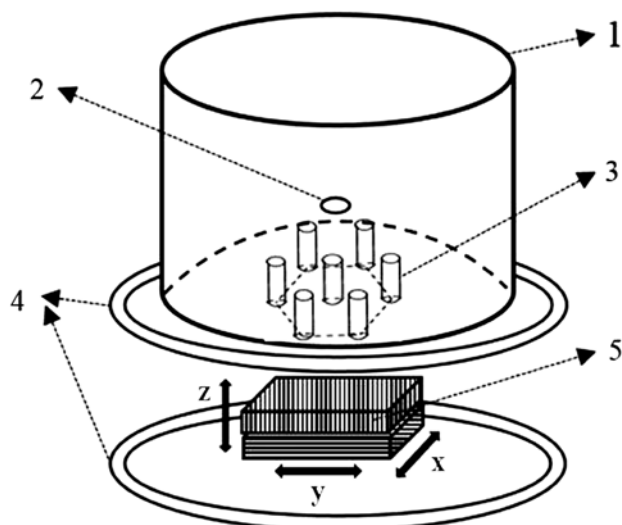
Materials and methods

Reagents

The studies described here used Fe_3O_4 NPs from two sources: 25-nm and 30-nm carboxylic acid-functionalized (SHP series) and 25-nm PEG-functionalized NPs (SPP series) were purchased from Ocean NanoTech (San Diego, CA, USA). In addition, 25-nm carboxylic acid-functionalized PrecisionMRX™ NPs manufactured in-house (Senior Scientific LLC, Albuquerque, NM, USA) were tested. Chemicals used included the following: N-hydroxysulfosuccinimide (Sulfo-NHS) and 1-ethyl-3-[3-dimethylaminopropyl]carbodiimide hydrochloride (EDC), purchased from Pierce (Rockford, IL, USA); bovine serum albumin, sodium azide, potassium ferrocyanide, sodium bicarbonate (NaHCO_3)

and ethylene diamine tetra-acetic acid (EDTA) purchased from Sigma-Aldrich (St. Louis, MO, USA); 1× phosphate-buffered saline, pH 7.4 (PBS) purchased from Gibco-BRL (Rockville, MD, USA); fetal bovine serum (FBS) purchased from HyClone (Logan, UT, USA). Anti-Her2 antibody was purchased from Bender MedSystems (now part of eBioscience, Inc., San Diego, CA, USA), and anti-CA125 antibody was purchased from QED Bioscience (San Diego, CA, USA).

SPMR measurements

A schematic diagram used in the SPMR experiments described here is shown in Figure 1, and a drawing of the equipment is shown in Figure 2. The SQUID sensor system is contained within a liquid helium Dewar and consists of seven-channel, second-order axial gradiometers that are inductively coupled to the SQUIDs (BTi 2004; 4D-Neuroimaging, San Diego, CA, USA). Helmholtz magnetizing coils with a diameter of 65 cm and 100 turns, aligned along the central axis of the sensor array, powered by a 5-kW current-regulated supply (Sorenson SGA 80/63, San Diego, CA, USA) orient the total magnetization vector of the NP ensemble along the z-axis of the sensor system during the pulse and before the decay begins. The magnetizing pulse is typically 4 mT and is applied for 0.75 s. To allow induced currents in the components of the SQUID sensor array and the environment to decay following the magnetizing pulse, a delay of 35 ms was incurred before turning on the SQUID sensors, followed by a measurement of the decaying magnetic field from the NPs for 2.2 s [2, 9]. To increase the signal-to-noise ratio, this sequence was repeated ten times, and the result signal averaged. A non-magnetic stage is used to move the SPMR source and to obtain additional field measurement points. The position of the stage is monitored by an optical position readout to keep track of the source's coordinates. A minimum of four field measurements are required to determine the x, y, z coordinates and magnitude of the source. The

SPMR data obtained from the SQUID control circuitry were digitized using a National Instruments PXI − 8336 platform equipped with a multichannel 16-bit digitizer (National Instruments Corporation, Austin, TX, USA), sent to a computer interface through a fiber-optic cable and read by a data acquisition software program written locally using a version of C language (CVI, National Instruments). This program controlled the pulsing sequence for the magnetizing coils and the SQUID electronics and provided a display of the data for monitoring purposes. Data analysis was performed using a multi-source analysis program, also developed using CVI. This code removes 60-Hz line contamination and other artifacts and provides signal-averaging. Additionally, the code compensates for background fields arising from the induced currents due to the magnetic field pulse by subtracting background data (acquired with no sample) from the sample data. The resulting relaxation curves are fit by a logarithmic function at long times to correct for DC offsets and an exponential function used to extrapolate to the time when the magnetizing field is turned off, to obtain the magnetic field amplitude at each sensor position [9]. To obtain the locations and source strengths of samples under the system, a modeling approach is used as, in general, the inverse problem for magnetic fields cannot be solved uniquely in three dimensions. The spatial distribution of the measured magnetic fields is modeled as the sum of one or more magnetic dipoles. The resulting fields calculated by these dipoles are compared to the measured fields with a least-squares algorithm, using the Levenberg-Marquardt algorithm, to obtain the x, y, z coordinates and the magnetic moments of the underlying sources. The solution for the inverse problem in this situation is simplified because the direction of the magnetic dipoles induced in the sources is parallel to the applied magnetizing field. Thus, the vector direction of the magnetic moments can be uniquely determined, requiring only four sensor positions per source. This alignment, and the reduction of the required parameters to solve the inverse problem, results in increased precision in determining the spatial coordinates of the sources. A resolution of 0.5 mm for reasonably large magnetic moments located several cm from the sensor system can be achieved with 95% confidence limits.

NP characterization

In addition to SPMR measurements of the NPs, DC SQUID susceptometry, transmission electron microscopy (TEM), and small-angle X-ray scattering (SAXS) of 25-nm Ocean NanoTech SHP and 25-nm PrecisionMRX™ NPs were performed.

DC susceptometry

Magnetization measurements were collected using a Quantum Design MPMS-7 SQUID magnetometer (Quantum Design, San Diego, CA, USA). Samples were prepared by depositing a small amount of the synthesized NPs suspended onto the end of a Q-tip® cotton swab (Unilever, Trumbull, CT, USA). High field magnetization curves were recorded from -5T to +5T (-4000 kA/m to +4000 kA/m) at 293 K. Low field magnetization was recorded from 0 to +6 mT (0 kA/m to 4.77 kA/m). The precise iron mass of each sample was determined destructively by heating the Q-tip™ in a 600°C furnace for 1 h to incinerate the organic material and then dissolving the iron-containing residue in hydrochloric acid. A phenanthroline/Fe^{2+} complex was formed in solution and spectrophotometrically quantified using the

Figure 2: MRX experimental setup.
(1) LiHe Dewar; (2) optional superconducting quantum interference detectors (SQUID) magnetometer channel (SQUID sensor not shown); (3) seven-channel second-order SQUID gradiometers (SQUID sensors not shown); (4) Helmholtz coil; (5) manually controlled non-magnetic 3D stage with optical readout.

concentration of a known dilution [3, 13]. The field-dependent magnetization data was normalized to the mass of iron in the sample to determine the saturation magnetization (σ_{sat}).

TEM and SAXS

Bright field TEM studies of synthesized NPs were performed using a JEOL 1200EX TEM operating at 120 kV (JEOL USA, Inc., Peabody, MA, USA). Size analysis of imaged particles was performed using ImageJ software [19]. The size distribution was calculated by deriving the particle diameter from the measured cross-sectional area (effectively assuming a spherical morphology) and calculating a number average and volume average diameter. SAXS was used for ensemble measurements of particle size and the corresponding size distribution. For this measurement, a concentrated solution of particles suspended in hexanes was injected into a glass capillary tube and analyzed using a Rigaku SmartLab diffractometer system with the SmartLab guidance system control software (Rigaku Technologies, Austin, TX, USA). Cu-K-alpha radiation (40 kV, 44 mA) was used in transmission geometry with a scintillation detector. Data analysis was performed using Rigaku NANO-Solver v. 3.5 software, assuming a spherical particle shape, a Gaussian distribution of particle sizes and calculating a volume average diameter.

Antibody conjugation of NPs

The carboxylate functionality of the polymer-encapsulated NPs allows straightforward, non-directional conjugation of amine groups on the antibodies to the carboxylate anions on the surface of the NPs using standard two-step EDC/NHS chemistry. Briefly, 1 mg of Ocean NanoTech NPs or 1 mg of PrecisionMRX™ NPs were suspended in double distilled water (ddH$_2$O). Sulfo-NHS and EDC were prepared fresh in 25-mg/ml solutions each. One hundred μl of each solution was added to the NPs and incubated at room temperature with shaking for 20 min. The pH of the solution was then adjusted to pH 8.5 with 50 mM NaHCO$_3$, 50 μg of antibody was added, and the solution was incubated at room temperature with shaking for 2 h. The NPs were purified from the reagent solution by centrifugation and resuspension in ddH$_2$O. The NP concentration was determined by performing a colorimetric iron assay as described previously. Antibody-conjugated NPs were stored at 4°C prior to use.

Cell lines

NIH:OVCAR-3, SKOV3, CHO, MDA-MB-231 and LNCaP cells were purchased from American Type Culture Collection (ATCC). MCF7/Her218 231 cells engineered to overexpress the Her2 receptor were a kind gift from Mien-Chie Hung (University of Texas M.D. Anderson Cancer Center). NIH:OVCAR-3 cells were cultured in RPMI 1640 medium supplemented with 10 mM HEPES, 2 mM L-glutamine, 1 mM sodium pyruvate, 4.5 g/l glucose, 1.5 g/l sodium bicarbonate, 0.01 mg/l bovine insulin, 20% FBS, 1% penicillin/streptomycin (v/v) and 4 μg/ml Ciproflaxacin. CHO cells were cultured in DMEM with 10% FBS, SKOV3 cells were cultured in Macoy's 5A medium with 20 mM L-Glutamine 1% penicillin/streptomycin and 10% FBS. LNCaP cells were cultured in RPMI1640 medium with 10% FBS and 1% penicillin/streptomycin. MCF7/Her2-18 cells were cultured in advanced Dulbecco's modified Eagle's medium/F-12 medium supplemented with 10% FBS, 1%

penicillin/streptomycin (v/v) and 4 μg/ml ciprofloxacin. MDA-MB-231 cells were cultured in Leibovitz's L-15 medium supplemented with 10% FBS, 1% penicillin streptomycin (v/v), and 4 μg/ml ciprofloxacin. All cell lines were cultured in an incubator at 37°C with 5% CO$_2$.

Cell binding assay

Cell lines were harvested with EDTA and washed with sterile PBS. Harvested cells were counted using 0.4% Trypan Blue solution on a hemocytometer. Each sample consisted of 3×10^6 cells suspended in 200 μl of cold PBS to which 15 pmol of conjugated NPs were added. Samples in 1.5-ml microcentrifuge tubes were centered under the SPMR instrument and placed below the center sensor. Cells and conjugated NPs were incubated for 15 min underneath the SPMR instruments and measurements were taken every 2 min starting at 1-min post NP addition.

In vivo delivery of conjugated NPs

NOD SCID or athymic nude female mice were purchased from Harlan Sprague Dawley. Two to 7 days prior to injection of cells, mice were implanted with a 17b-estradiol pellet (1.7 mg, 60-day release). MCF7/Her218 cells (7×10^6) or SKOV3 (3×10^6) cells were injected with 0.150-ml of Matrigel™ into each hind limb flank. Mice were used when tumors reached approximately 1 cm in diameter. NOD SCID mice implanted with MCF7/Her218 tumors were injected retro-orbitally with anti-Her218-conjugated 25-nm Ocean NanoTech SPP NPs at 5 mg NP/kg body mass. An athymic nude mouse implanted with an SKOV3 tumor was injected in a similar fashion with folic-acid-conjugated PrecisionMRX NPs at 10 mg NP/kg body mass. Mice were placed in the SPMR instrument and imaged at five stage positions and successive time points following injection of NPs. At the end of the measurements, the mice were terminated, and organs (tumor, lungs, liver, spleen, kidneys and heart) were excised and their magnetic moments measured in the SPMR instrument.

Results

NP characterization

DC susceptometry

Magnetization curves of 25-nm Ocean NanoTech SHP and 25-nm PrecisionMRX™ NPs at 293 K are plotted in Figure 3. High field magnetization curves plotted in Figure 3A show that the σ_{sat} of the PrecisionMRX™ NPs is 101 A·m^2/kg Fe, nearly twice the saturation value of the Ocean SHP NPs of 53.4 A·m^2/kg Fe. If the particles are assumed to be composed completely of Fe$_3$O$_4$, the normalized σ_{sat} of PrecisionMRX™ NPs is 73.9 A·m^2/kg Fe$_3$O$_4$, and the Ocean SHP NPs is 38.6 A·m^2/kg Fe$_3$O$_4$, 80% and 42% of bulk Fe$_3$O$_4$ at 293 K, respectively [6]. At low fields, the magnetization
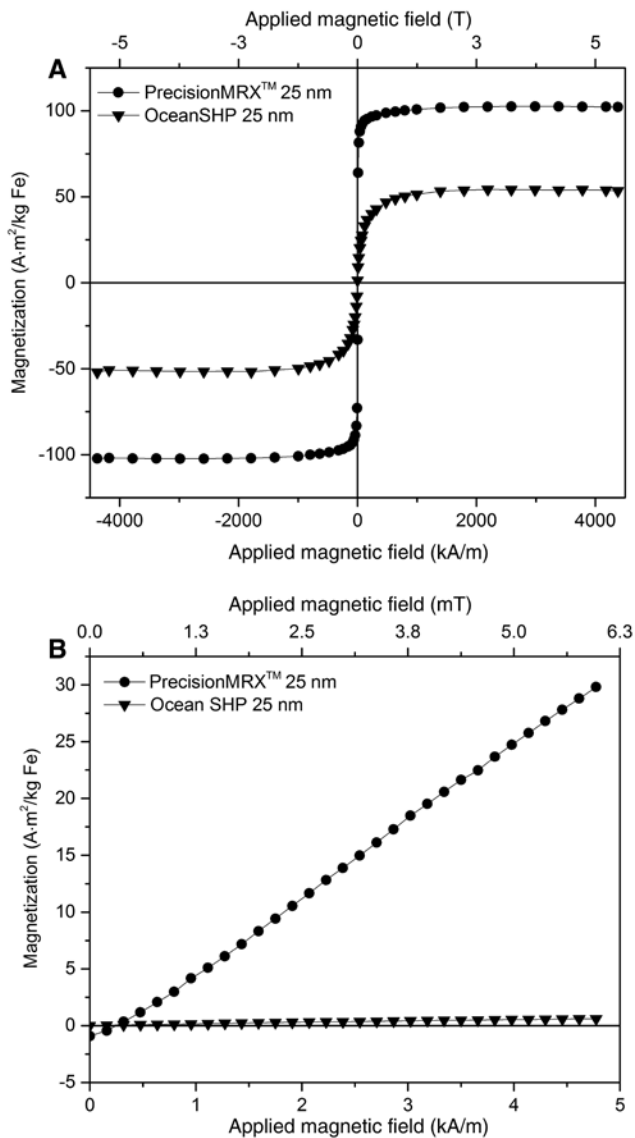
Figure 3: DC susceptometry measurements.
(A) Magnetization curves of Ocean SHP 25-nm nanoparticles (NPs) at high fields show that the σ_{sat} of PrecisionMRX™ NPs is 101 A·m²/kg Fe, nearly twice the saturation value of the Ocean SHP NPs of 53.4 A·m²/kg Fe. (B) At low fields, the magnetization of the PrecisionMRX™ NPs increase rapidly, reaching magnetization values approximately 30 times greater than the Ocean SHP at an applied field of 6 mT.

of the PrecisionMRX™ NPs increases rapidly, reaching magnetization values approximately 30 times greater than the Ocean SHP at an applied field of 6 mT (Figure 3B).

TEM and SAXS

Representative TEM images of PrecisionMRX™ and Ocean NanoTech SHP 25-nm NPs are presented with accompanying
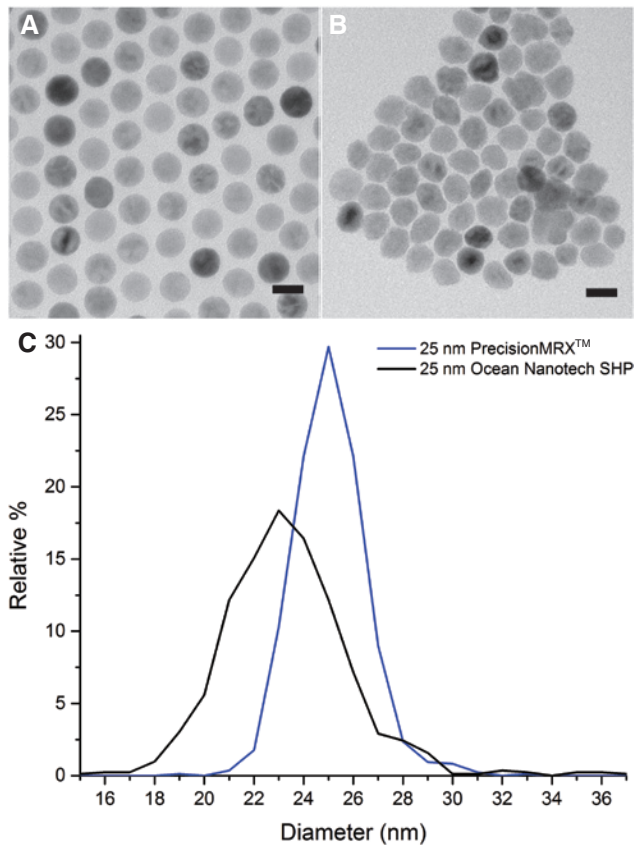

Figure 4: Transmission electron microscopy (TEM) images and analysis.
(A) PrecisionMRX™ 25-nm nanoparticles (NPs) with a mean size of 25.3 nm and a σ of 1.1 nm; (B) Ocean SHP 25-nm NPs with a mean size of 23.8 nm and a σ of 2.6 nm; (C) the accompanying TEM size distributions. Scale bars represent 25 nm.

size distribution histograms in Figure 4. TEM analysis of PrecisionMRX™ NPs (Figure 4A) confirms the formation of spherical particles with a number average particle diameter of 25.3 nm (σ=1.1 nm), a volume average diameter of 25.5 nm and a size distribution well described by a Gaussian curve. TEM analysis of Ocean NanoTech SHP NPs (Figure 4B) shows irregularly shaped particles with a number average particle diameter of 23.8 nm and a σ of 2.6 nm. SAXS measurements of PrecisionMRX™ NPs describe spherical particles with a volume average diameter of 24.5 nm (σ=1.5 nm). SAXS analysis of Ocean SHP resulted in a volume average diameter of 23.1 nm (σ=2.9 nm), in good agreement with the results of the TEM analysis.

Cell incubations

To demonstrate specific binding of antibody-conjugated NPs to cells, several cell incubation studies were
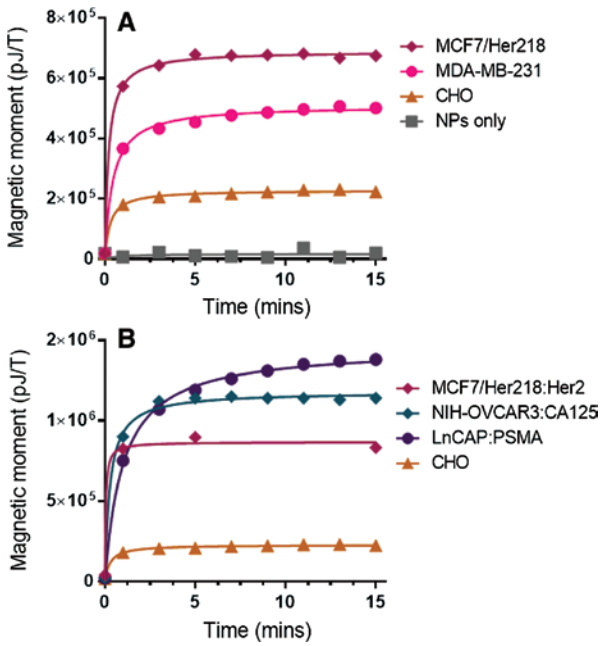
Figure 5: Detection of cell binding in the superparamagnetic relaxometry (SPMR) instrument using different cell lines and 25-nm Ocean Nanotech SPP nanoparticles (NPs).
(A) Comparison of binding of anti-Her2-conjugated 25-nm Ocean Nanotech NPs with cells lines with varying expression of the Her2 receptor. The measured magnetic moment increases with increasing expression of Her2, demonstrating specific binding as a function of receptor density. Adapted from [11]. (B) Comparison of different cancer cell lines incubated with their respective cancer specific markers; MCF7/Her218 is a breast cancer cell line incubated with Her2-conjugated NPs (a breast-specific cancer marker), NIH-OVCAR3 is an ovarian cancer cell line incubated with CA125-conjugated NPs (an ovarian-specific cancer marker), LnCAP is a prostate cancer cell line incubated with anti-PSMA-conjugated 30-nm Ocean Nanotech SHP NPs, CHO cells incubated with anti-Her2-conjugated 25-nm Ocean Nanotech SHP NPs (adapted from [11]) shown for comparison as a negative control.

performed. Previously, we showed that anti-Her2-conjugated NPs specifically bind cells expressing Her2 on the surface [11]. Furthermore, we demonstrated that the magnetic moment signal correlates to the levels of Her2 expressed at the cell surface [1]. To illustrate, Figure 5A shows the results of a 15-min incubation of anti-Her2-conjugated Ocean Nanotech SHP NPs with a series of breast cancer cell lines that express Her2 to varying degrees, with MCF7/Her218 having the highest expression, MDA-MB-231 having reduced expression and Chinese hamster ovary (CHO) cells as a negative control. A background measurement of NPs alone was taken (time=0) prior to the addition of cells. The measured SPMR signal increased sharply following the addition of cells to the NP solution (t=1 min), with a maximum SPMR signal reached after 5 min of

incubation. MCF7/Her2-18 cells demonstrated the highest relaxometry signal (7.00E+05 pJ/T), MDA-MB-231 had an intermediate relaxometry signal (4.35E+05 pJ/T), CHO had a low maximal relaxometry signal (2.68E+05 pJ/T) and NPs in media alone demonstrated a minimal background signal (2.9E+04 pJ/T). The solid lines in Figure 5A are a theoretical fit to the data using the following rate equation:

$$\frac{d\rho}{dt} = \alpha(\rho_{so}-\rho)(\rho_{no}-\rho) \qquad (1)$$

Eq. 1 describes the change in density of NPs (ρ) bound to the cell, where so refers to the number of available sites on a cell and no the number of available NPs. At t=0, there are no NPs bound to the cell, whereas the density of NPs on the cell reaches saturation at time t with a rate constant α. Integrating Eq. 1 provides the density of NPs per cell, which in turn reflects the specific binding of NPs to each cell line. Table 1 contains the results of these fits, indicating that the relative specificity for the anti-Her2-conjugated NPs for these cell lines is: 1.0:0.69:0.31. These measurements are similar to results obtained by flow cytometry [11].

To illustrate that SPMR is not limited to detection of Her2-positive breast cancer cells, additional experiments were conducted using MCF7/Her218 cells, as well as ovarian and prostate cancer cell lines. In a manner similar to the studies described above, MCF7/Her218 cells were incubated with anti-Her2-conjugated 25-nm Ocean Nanotech SHP NPs. NIH-OVCAR3, ovarian cancer cells expressing the CA125 glycoprotein, were incubated with anti-CA125-conjugated 25-nm Ocean Nanotech SHP NPs. LNCaP, prostate cells that express prostate-specific membrane antigen (PSMA), were incubated with anti-PSMA-conjugated 30-nm Ocean Nanotech SHP NPs. The results of these incubations are plotted in Figure 5B. For comparison, the results from the incubation of

**Table 1:** Results of a theoretical fit to the incubation data of Figure 1 top.

Cell line	NP #	NP/Cell	R(MCF7)
MCF7/Her218	4.37E+12	5.83E+05	1
MDA-MB-231	3.00E+12	4.00E+05	0.69
CHO	1.37E+12	1.82E+05	0.31
None[a]			0.03

NP #, total number of nanoparticles (NPs) bound to the 7.5 million cells; NP/cell, ratio of NPs to cells; R(MCF7), ratio of NPs/cell compared to the MCF7/Her218 cell line or a measure of the relative specificity. [a]No cells were present.

CHO cells with anti-Her2-conjugated NPs are included as a negative control (adapted from [11]). As with the prior study, the measured SPMR signal increases from the background level (NPs only) following the addition of cells. The signal reaches a maximum after approximately 5 min of incubation (15 min for LNCaP cells) and plateaus, indicating saturation of available binding sites by conjugated NPs.

An additional series of cell studies was performed to characterize the performance of PrecisionMRX™ NPs in SPMR experiments. To optimize the number of NPs used in an *in vitro* experiment, NP titrations were performed by measuring the MRX signal of a range of concentrations of anti-Her2-conjugated NPs. Dilutions of the NPs in 1X PBS buffer, pH 7.4, were prepared (7.5 picomoles to 0.75 picomoles). To each solution, 1×10^6 MCF7/Her2-18 cells were added. A saturation curve of signal vs. NP concentration results is shown in Figure 6A. From this study, a quantity of NPs eliciting a signal at the high end of the linear range of detection (~2 pmole) would be deemed optimal for cell titration studies where NPs are not present in quantities to saturate all binding sites on cells. A larger quantity of

NPs (4 picomoles or greater) would be used in an experiment where NPs are desired in large excess. Cell titrations were performed with PrecisionMRX™ NPs to determine the lower limit of cell detection using a fixed quantity of conjugated NPs. Serial dilutions of MCF7/Her2-18 cells (125×10^3–15.6×10^3 cells) were incubated for 15 min with 1.5 pmole of anti-Her2 conjugated NPs. In Figure 6B, a lower limit of detection of approximately 15×10^3 cells is shown. A cell incubation experiment using 1.5 pmole anti-Her2-conjugated NPs combined with 1×10^6 MCF7/Her2-18 cells is shown in Figure 6D. A typical saturation curve results, with a rapid increase in the detected moment following addition of cells to the NPs, with a plateau occurring after approximately 5 min, indicating maximum NP binding. In a final experiment to determine the lower limit of NP detection *in vivo*, known quantities of unconjugated NPs were injected subcutaneously into an athymic nude female mouse, which was immediately analyzed in the SPMR instrument. The results in Figure 6D demonstrate a linear relationship between NP concentration and magnetic moment, with a lower detection limit of 1.5 pmole NPs, in agreement with the *in vitro* results.
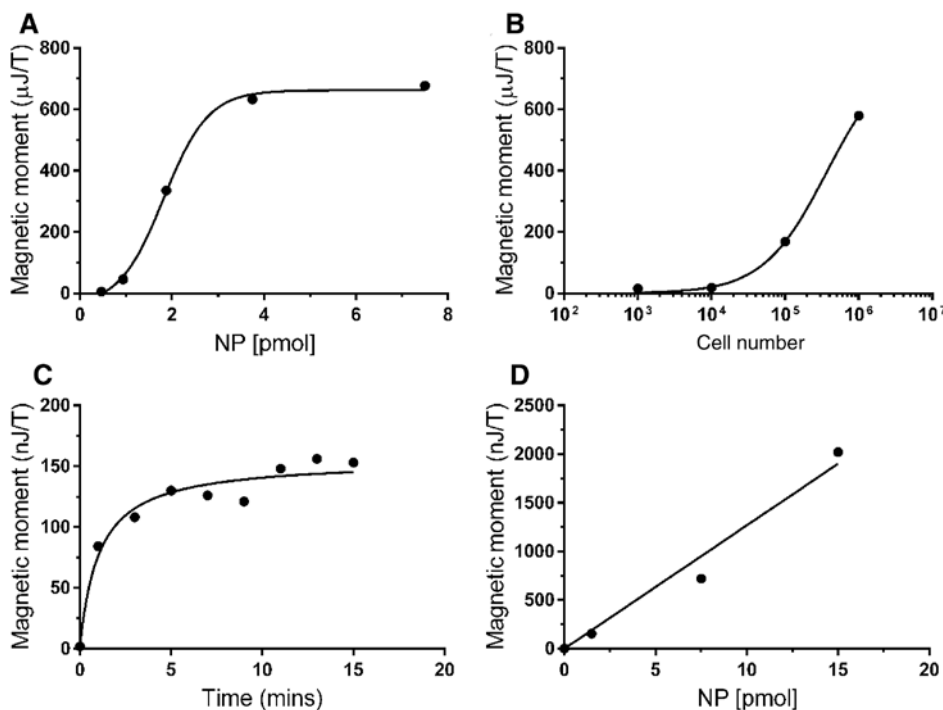
Figure 6: Biological characterization of the PrecisionMRX™ nanoparticles (NPs) *in vitro* and *in vivo*.
(A) NP titration using varying amounts of anti-Her2-conjugated NPs and incubated with 1×10^6 MCF7/Her218 cells. (B) Cell titration using anti-Her2-conjugated NPs (1.5 pmole) and incubated with varying amounts of MCF7/Her218 cells. (C) Cell incubation using anti-Her2-conjugated NPs (1.5 pmole) and incubated with 1×10^6 MCF7/Her218 cells. (D) *In vivo* NP titration, varying amounts of unconjugated NPs were injected subcutaneously into nude mice and immediately analyzed in the superparamagnetic relaxometry (SPMR) instrument. A magnetic moment was detected with as few as 1.5 pmole of NPs. Solid lines on plots are shown as a guide.

A

B

C
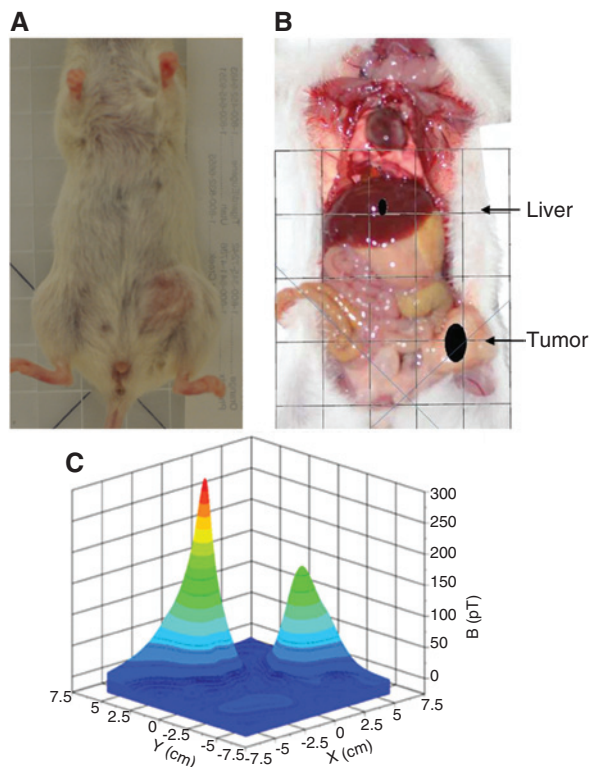
Figure 7: Example of *in vivo* data gathered from the superparamagnetic relaxometry (SPMR) instrument.
(A) Female mouse being prepared for analysis in the SPMR system; an MCF7/Her2-18 tumor has grown on the left flank. (B) Overlay of image of dissected mouse with the location of two sources as determined by the SPMR software; the two sources correspond to the liver and the tumor. (C) Contour plot of the magnetic fields measured for the mouse in (A).

SPMR in animal models of cancer

SPMR has been used to identify tumors *in vivo* in animal models. An example of this procedure using an NOD SCID mouse with an MCF-7/Her2-18 xenograft tumor is shown in Figure 7. The mouse was given a retro-orbital injection containing 50 µl of anti-Her2-conjugated 25-nm Ocean Nanotech SPP NPs. Figure 7A is a photograph of the mouse before placement in the SPMR instrument showing a tumor on the inner lower right flank of the animal. Figure 7B shows the dissected mouse with the locations of the two measured dipole sources superimposed on it. The filled spots indicate the center of mass of the measured magnetic moment, with the size of the spot reflecting the relative accuracy of location (a smaller spot reflects higher accuracy of location). In Figure 7B, the smaller spot is superimposed on the liver, whereas the larger spot aligns with the position of the tumor. Figure 7C shows the magnetic field map contour fit, with two prominent peaks corresponding to the liver and the tumor. The detected magnetic moment (pT) is largest in the liver, indicating that the majority of NPs have been taken up by the reticuloendothelial system (RES). The smaller peak is the result of NPs that have accumulated in the tumor. No other organs in the mouse were detected in the SPMR measurement, nor did later measurement of individual organs result in a measurable magnetic moment.

In addition to specific detection *in vivo*, using the known amount of NPs (and thus, Fe) injected into the subject, the percentage of injected material delivered to the tumor is obtained. In general, this is a difficult measurement to make *in vivo* by other techniques and is normally done following *ex vivo* measurements of the extracted tumor. As SPMR measures the magnetic moments of only the bound NPs, measurements of the amount of bound NPs in the tumor are possible. This can be of great value in determining the efficacy of drug delivery as well as measurement of the effectiveness of stealth coatings on NPs to increase their circulation time. The experiment performed with the mouse shown in Figure 7 was used to calculate the efficiency of delivery of NPs to a breast cancer tumor. The injected material was measured to contain 2.9 mg/ml of Fe, yielding 0.145 mg of injected Fe. Experience has shown that a cotton tip can be used to measure accurately the magnetic moment per µl of dried NPs [11]. A SPMR measurement of a cotton tip with the same quantity of NPs gives a value of 1.42×10^5 pJ/T, yielding a moment per mass of 4.90×10^6 pJ/T/mg of Fe. The magnetic moment observed for the tumor in Figure 7 was 2.0×10^4 pJ/T, corresponding to 2.1% of the injected NPs attaching to the MCF7 cancer cells in the tumor; ~17% ended up in the liver with the rest dispersed through the animal and not observable.

The SPMR method can be used to identify a number of sites within an athymic nude female mouse with an SKOV3 (ovarian cancer) xenograft tumor. The mouse was retro-orbitally injected with folic acid-conjugated Precision-MRX™ NPs. Folic acid targets the tumor, along with many other tissues in the body expressing the folic acid receptor. The purpose of the experiment was to demonstrate that multiple sources, representing NPs bound to different tissues, could be sensitively detected. Figure 8 shows that four peaks, corresponding to four unique sources, were detected when measuring the mouse following NP injection. This result was expected, as the conjugated NPs will bind specifically to tissues actively metabolizing folic acid. This preliminary result indicates that the SPMR method can successfully locate a number of sources within one animal, though there remains a possibility that two sources lying sufficiently close to each other cannot be accurately resolved by the inverse solution.
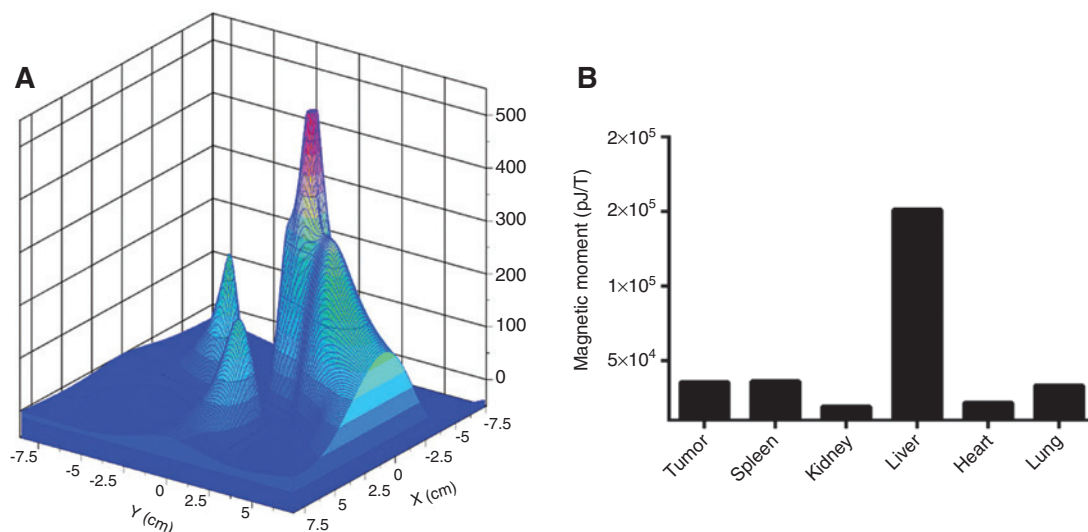
Figure 8: Contour plot of a mouse with multiple dipole sources.
(A) Contour plot of magnetic fields resulting from superparamagnetic relaxometry (SPMR) measurements in a mouse injected with folic-acid-conjugated PrecisionMRX™ nanoparticles (NPs); four distinct peaks were resolved corresponding to the liver, the tumor, the spleen and the kidneys. (B) The magnitudes of the measured moments per organ.

Discussion

Advances in SQUID sensor technology

The results presented in this paper studies were performed using the SQUID-based system presented in Figure 2. Since the accomplishment of these studies, several important improvements were introduced. We have substituted our regular DC SQUIDs with devices that have integrated cryoswitch, effectively decoupling the sensors from gradiometers' pick-up during the magnetizing pulse, an improvement that ensures fast recovery of the SQUIDs. A new, non-magnetic computer-controlled 3D stage with a readout of 0.1-mm accuracy was implemented, thus significantly shortening the acquisition time for scanning large objects. We have added a feedback to SQUID's gradiometer channels from a single SQUID magnetometer. The feedback and cryoswitches to the SQUIDs allowed for reduction of the dead time from 35 ms to <20 ms. These improvements led to better determination of the magnetic fields measured by the sensors when extrapolating toward the end of the magnetizing pulse. The feedback partially compensates for the effects of magnetic ringing originating from the induced currents in the conductive components of the environment. This allows the system to be used to its full potential not only in unshielded environments that are clean of metal, but also in buildings with significant metal infrastructure (hospitals, research centers, etc.).

PrecisionMRX™ NPs improve sensitivity of SPMR measurements

Characterization of PrecisionMRX™ NPs demonstrated improved properties (size/shape dispersity, magnetism) with respect to commercially available NPs. The significance of these enhancements is the increased sensitivity of the SPMR measurements *in vitro* and *in vivo*. This is accomplished by increasing the number of NPs that attach to cells whose size gives decay constants that fall within the SPMR time windows. Measurements of the number of NPs per cell, compared to the number of sites available for a given Ab for all previously available NPs, indicate that if all sites are occupied by NPs, the majority of these do not give decay times falling within the SPMR window. Typically 1–2% of the NPs on the cell were observed for these NPs. The narrow distribution of the PrecisionMRX™ increases this percentage by a factor of three or more in initial experiments.

Increased sensitivity for detecting and localizing cancer

The combination of improved SQUID sensor performance using background sensors with feedback along with the improved size distributions of the NPs has increased the sensitivity for detecting cancer by orders of magnitude over our previous SPMR measurements. This increase in

sensitivity is coupled with automatic stage positioning of animals during pre-clinical experiments. Animal experiments now can be accomplished using over-sampling measurements that increase the accuracy of localization of multiple tumors in the animal models, permitting a greater diversification of cancer studies, both to determine specificity as well as to provide a model for cancer therapy monitoring.

Conclusions

The results presented here show that SPMR technology can be used to specifically identify different types of Ab and cancer cell lines through incubation measurements. These same measurements also show that unbound NPs do not give a SPMR signal falling in the measurement time window. The measured sensitivity for breast cancer cells is orders of magnitude greater than a mammogram, and the specificity of the conjugated NPs is such that benign tumors will not be targeted. These facts, along with the observation that the decaying magnetic fields are transparent to tissue and bone and that the observed magnetic moments are linear with cell number, make SPMR an ideal method for application to cancer detection and treatment monitoring. Using PrecisionMRX™ NPs, a lower detection limit of 10,000 cells was measured *in vitro* at a distance of 4.5 cm from the detector. This represents an improvement of 2 orders of magnitude in the detection sensitivity of SPMR achieved with commercially available NPs reported previously [11].

The ability to detect human cancer cells in animal models with great sensitivity is a precursor to taking SPMR methods to human tumor detection and localization. The results of these pre-clinical animal experiments are necessary to proceed toward approval of human subjects. The measured high sensitivity with the new NPs and SQUID sensors indicates that clinical applications of SPMR will have a high impact. The localization capability measured in the animal model also indicates that tumors can be localized in clinical settings sufficiently accurately for therapeutic applications.

References

[1] Adolphi NA, Butler KS, Lovato DM, et al. Imaging of Her2-targeted magnetic nanoparticles for breast cancer detection, comparison of SQUID-detected magnetic relaxometry and MRI. Contrast Media Mol Imaging 2012; 7: 308–319.

[2] Adolphi NL, Huber DL, Bryant HC, et al. Characterization of single-core magnetite nanoparticles for magnetic imaging by SQUID relaxometry. Phys Med Biol 2010; 55: 5985–6003.

[3] American Society for Testing and Materials. Standard test method for iron in trace quantities using the 1,10-phenanthroline method. West Conshohocken: ASTM Standard 2000; E394–E409.

[4] Brenner D, Williamson SJ, Kaufman. Visually evoked magnetic fields of the human brain. Science 1975; 190: 480–482.

[5] Cohen D. Magnetoencephalography: evidence of magnetic fields produced by alpha-rhythm currents. Science 1968; 161: 784–786.

[6] Cullity BD, Graham CD. Introduction to magnetic materials. Picataway: Wiley-IEEE Press 2009.

[7] Dolgovskiy V, Lebedev V, Colombo S, et al. A quantitative study of particle size effects in the magnetorelaxometry of magnetic nanoparticles using atomic magnetometry. J Magn Magn Mater 2015; 379: 137–150.

[8] Eberbeck D, Wiekhorst F, Steinhoff U, et al. Specific binding of magnetic nanoparticle probes to platelets in whole blood detected by magnetorelaxometry. J Magn Magn Mater 2009; 321: 1617–1620.

[9] Flynn ER, Bryant HC. A SQUID based system for in-vivo cancer imaging. Phys Med Biol 2005; 50:1273–1293.

[10] Hämäläinen M, Hari R, Ilmoniemi RJ, Knuutila J, Lounasmaa OV. Magnetoencephalography – theory, instrumentation, and applications to noninvasive studies of the working human brain. Revs Mod Phys 1993; 65: 413–497.

[11] Hathaway HJ, Butler KS, Adolphi NA, et al. A novel method for early detection of breast cancer using magnetic nanoparticles and ultra-sensitive magnetic field sensors. Breast Cancer Res 2011; 13: R108.

[12] Huang M, Aine CJ, Supek S, Best E, Ranken D, Flynn ER. Multi-start downhill simplex methods for spatio-temporal source localization in magnetoencephalography. Electroenceph Clin Neurophys 1998; 108: 32–44.

[13] Huber DL, Venturini EL, Martin JE, et al. Synthesis of highly magnetic iron nanoparticles suitable for field structuring using a [beta]-diketone surfactant. J Magn Magn Mater 2004; 278: 311–316.

[14] Johnson C, Adolphi NL, Butler KL, et al. Magnetic relaxometry with an atomic magnetometer and SQUID sensors on targeted cancer cells. J Magn Magn Mater 2012; 324: 2613–2619.

[15] Knappe S, Sander TH, Kosch O, Wiekhorst F, Kitching J, Trahms L. Cross-validation of microfabricated atomic magnetometers with superconducting quantum interference devices for biomagnetic applications. Appl Phys Lett 2010; 97: 133703.

[16] Kotitz R, Weitschies W, Trahms L, Semmler W. Investigation of Brownian and Neel relaxation in magnetic fluids. J Magn Magn Mater 1999; 201: 102–104.

[17] Ludwig F, Mäuselein S, Heim E, Schilling M. Magneto-relaxometry of magnetic nanoparticles in magnetically unshielded environment utilizing a differential fluxgate arrangement. Rev Sci Instr 2005; 76: 10610.

[18] Neel L. Some theoretical aspects of rock-magnetism. Adv Phys 1955; 4: 191–243.

[19] Rasband WS. ImageJ. 1997–2012. Bethesda: US. National Institutes of Health.

[20] Zimmerman JE. Macroscopic quantum interference effects through superconducting point contacts. Phys Rev 1966; 141: 367–375.